Author Query Form

Journal Title: Journal of Mechanical Engineering Science, Proceedings of the Institution of Mechanical Engineers Part C [PIC]

Article Number: 476232

Dear Author/Editor,
Greetings, and thank you for publishing with SAGE. Your article has been copyedited and typeset, and if we have any queries for you they are listed below. Please address these queries when you return your proof corrections. Thank you for your time and effort.

Please ensure that you have obtained and enclosed all necessary permissions for the reproduction of artistic works, (e.g. illustrations, photographs, charts, maps, other visual material, etc.) not owned by yourself, and ensure that the Contribution contains no unlawful statements and does not infringe any rights of others, and agree to indemnify the Publisher, SAGE Publications Ltd, against any claims in respect of the above warranties and that you agree that the Conditions of Publication form part of the Publishing Agreement.

Any colour figures have been incorporated for the on-line version only. Colour printing in the journal must be arranged with the Production Editor, please refer to the figure colour policy outlined in the e-mail.

Please assist us by clarifying the following queries:

1. The references have been renumbered for sequence. Please verify for correctness.
2. Please verify whether Kim et al. has to be set as a reference.
3. Please verify t for correctness..
4. There is a mismatch between the author names in the text and the list for reference [4]. Please verify.
5. Please check 'si' in equation (3) for correctness.
6. Please check 'of or 1 h' for correctness.
7. Figures 5 and 6 have not been cited in the text. Based on the figure captions, Figures 1, 4, and 3 under 'Experimental procedure' have been changed as Figures 4, 5, and 6, respectively. Please verify for correctness.
8. 'mm/mn' has been changed as 'm/min'. Please verify for correctness.
9. Please verify the sentence "It believes inversely with the…" for clarity.
10. Please verify the sentence "In this article, we proposed …" for clarity.
11. References [2] and [31] [manuscript nos] and [20] and [23] are duplicate references and hence have been deleted. Please check.
12. Please provide the date and location for reference [21].
13. References [50] to [54] are not cited, but listed. Please check.
14. Table 1 is given with two captions. The table which corresponds to the text has been taken. Also, 12NC6 has been set as 12NiCr6. Please verify.

Institution of MECHANICAL ENGINEERS

Journal of MECHANICAL ENGINEERING SCIENCE

Original Article

Proc IMechE Part C:
J Mechanical Engineering Science
0(0) 1–13

DOI: 10.1177/0954406213476232
pic.sagepub.com
SAGE

A numerical analysis of relationship between ductility and nucleation and critical void volume fraction parameters of Gurson–Tvergaard–Needleman model

M Hadj Miloud[1,2], A Imad[3], N Benseddiq[3], B Bachir Bouiadjra[4], A Bounif[2] and B Serier[4]

Abstract

Gurson–Tvergaard–Needleman model is widely used to describe the three stages of ductile tearing: nucleation, growth and the coalescence of micro-voids. The aim of this article is to study the relationship between volume fraction of voids and the fracture strain ε_f. The effects of the volume fraction of nucleation, f_N, and the critical volume fraction, f_c, were analysed. These parameters play crucial roles in the process of ductile damage. A phenomenological analysis is carried out to study the relationship between the different void volume parameters and the fracture strain ε_f. A method is proposed for the determination of f_N and f_c, knowing the experimental fracture strain ε_f. The experimental parameters are extracted from the load–diametric contraction curve of an axisymmetric notched tensile bar test AN2.

Keywords

Damage mechanics, Gurson model, parameters identification, parametric analysis

Date received: [redacted]; accepted: 3 January 2013

Introduction

Metallographic studies[1,2] demonstrate that ductile damage of a metal is basically characterised by three mechanisms of void growth: (a) nucleation of voids due to fracture of particle–matrix interface, failure of the particle or micro-cracking of the matrix surrounding the inclusion; (b) growth of voids leading to an enlargement of existing holes; and (c) coalescence or micro-cracks initiated from voids leading to the drop of the load-carrying capacity of the material, when the void volume fraction (VVF) approaches unity.

One of the best known micro-mechanical models describing the damage of metallic ductile materials
1 is that of Gurson.[3] Based on the works of Rice and Tracey[4] and McClintok,[5] Gurson further studied the plastic flow around voids in a metallic material.

The Gurson model was derived by assuming a homogeneous deformation field in the matrix surrounding the void. He developed a constitutive model for porous ductile media based on a rigid-plastic material behaviour and the upper bound theorem of plasticity. This model is based on detailed phenomenological studies of the bifurcation behaviour in materials with periodic distributions of cylindrical and spherical voids

$$\Phi(\Sigma, \bar{\sigma}, f) = \frac{\sigma_{eq}^2}{\bar{\sigma}^2} + 2f\cosh\left(\frac{3}{2}\frac{\sigma_m}{\bar{\sigma}}\right) - (1 + f^2) = 0$$

where σ_{eq} is the macroscopic equivalent von Mises stress and f the VVF considered as a damage parameter.

[1]Département de Mécanique, Université Hassiba Benbouali de Chlef, Chlef, Algérie
[2]Département de Mécanique, Université des Sciences et de la Technologie 'Mohamed Boudiaf' Oran, Algérie
[3]Laboratoire de Mécanique de Lille, UMR CNRS 8107, Cité Scientifique, France
[4]LMPM, Department of Mechanical Engineering, University of de Sidi Belabes, Sidi Belabès, Algéria

Corresponding author:
B Serier, LMPM, Department of Mechanical Engineering, University of de Sidi Belabes, Sidi Belabès 22000, Algéria.
Email: boualems@yahoo.fr

Tvergaard[6,7] refined the constitutive model by incorporating some additional parameters ($q_{1,}$ q_2), resulting in the following yield function

$$\Phi(\Sigma, \bar{\sigma}, f) = \frac{\sigma_{eq}^2}{\bar{\sigma}^2} + 2q_1 f^* \cosh\left(\frac{3}{2} q_2 \frac{\sigma_m}{\bar{\sigma}}\right) - (1 + q_1^2 f^* 2) = 0 \tag{1}$$

Note that Tvergaard has originally suggested the values of the additional parameters as $q_1 = 1{:}5$ and $q_2 = 1$. Perrin and Leblond[8] have determined a correlation between the parameter q and porosity fraction f: $q = q(f)$. These authors showed that when the porosity fraction tends to zero, the value of tends towards 1.47. Faleskog et al.[9] indicated that the two parameters ($q_{1,}$ q_2), depend on the material hardening exponent. Steglich and Brocks[10] have proposed a yield condition for nodular cast iron. The condition was determined from a cell model which results from using a quadratic
2 equation to estimate the parameter $q_{1.}$ Moreover, Kim et al. and Ragab[11] showed that the q parameters should be varied with the triaxiality of the stress field, as well as the initial porosity. Vadillo and Fernández-Sáez[12] used a consistent fully implicit integration of the constitutive equations of the Gurson–Tvergaard model with the assumption that the q parameters depend on the triaxiality and the initial porosity of the stress field. Dutta et al.[13] pro-
3 posed a new form for a spatial variation of t q_2 parameter near the crack tip using two additional parameters q_{2a} and q_{2b}, given by $q_2 = 1 + q_{2a} e^{-q_{2b}\rho}$, where $\rho = r/l_c$, r is the distance from the crack tip and l_c the characteristic length. The value of q_2 tends towards 1.2 near the crack tip and towards unity far from the crack tip. The matrix flow stress, $\bar{\sigma}$, can be obtained by enforcing equality between the rates of macroscopic plastic works and the matrix plastic work

$$\sigma_{ij} \dot{\varepsilon}_{ij}^p = (1 - f)\bar{\sigma}\dot{\bar{\varepsilon}}^p \tag{2}$$

where $\dot{\varepsilon}_{ij}^p$ is the macroscopic plastic strain rate tensor and $\dot{\bar{\varepsilon}}^p$ the average effective plastic strain rate of the material. It can be seen that the above equation recovers that of von Mises' in the limiting case of zero porosity ($f \to 0$).

The effective VVF f^* has been introduced by Needleman and Tvergaard[4] to better predict the
4 effect of void coalescence (Figure 1).

$$\Phi(\Sigma,\bar{\sigma},f) = \frac{\sigma_{eq}^2}{\bar{\sigma}^2} + 2q_1 f^* \cosh\left(\frac{3}{2} q_2 \frac{\sigma_m}{\bar{\sigma}}\right) - (1 + q_1^2 f^{*2}) = 0$$

5
$$f^*(f) = \begin{cases} f \ si\ f \leqslant f_c \\ f_c + \delta(f - f_c)\ si\ f_c < f < f_F \\ f_U^*\ si\ f \geqslant f_F \end{cases} \tag{3}$$

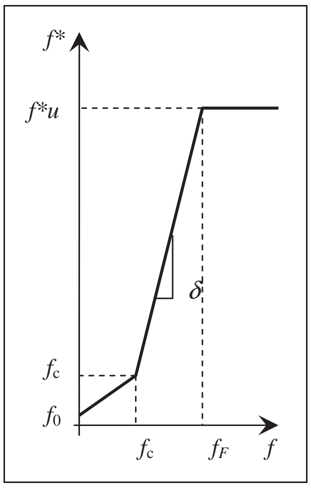

Figure 1. VVF evolution.
VVF: void volume fraction.

where δ, can be expressed as $\delta = \frac{f_U^* - f_c}{f_F - f_c}$, denotes the coalescence accelerator factor, where f is the current volume fraction of the voids; f_F and f_c denote, respectively, the VVFs at failure and the critical situation in which f starts to deviate from f^*; and f_U^* is the value of f^* at fracture condition (i.e. 2) (see figure) The load-carrying capacity vanishes when $f^* = 1/q_1\, f_U^* = 1/q_1$.

Generally, the initial VVF, f_0, is evaluated by microscopical examination of the undamaged material; it is a parameter that characterises the initial state of the material. The critical VVF, f_c, signifies the onset of coalescence. In most investigations, only the critical VVF, f_c, is considered as a material parameter, obtained by fitting the numerical calculations with the experimental results, and the other parameters are fixed arbitrary. According to Zhang and Niemi,[14] f_c is not constant but decreases when the stress triaxiality ratio T increases. However, other authors note that f_c can be taken as a constant only for small values of f_0. In a similar study, Steglich and Brocks[15] confirmed that the value of f_c depends on stress triaxiality T: f_c decreases with the increase of T.

They are several methods to determine the critical VVF f_c. One is using cell models developed by Koplik and Needleman,[16] Kuna and Sun[17] and Brocks et al.[18] This method is limited because it can be used only for a given initial VVF and it does not take into account the nucleation phase. The intermediate void nucleation process is very important in ductile fracture, and it is very difficult to incorporate into cell models. Sun et al.[19–21] have suggested that f_c can be numerically obtained from smooth axisymmetric tensile tests and then applied to a more general stress status case with the advantage of including the void nucleation.

Many authors have used the classical best fit methods to calibrate f_c by combining notched tensile bar tests and finite element (FE) analyses.[22–25]

Zhang et al.[26] and Acharyya[27] determined f_c using a physical micro-void coalescence criterion based on

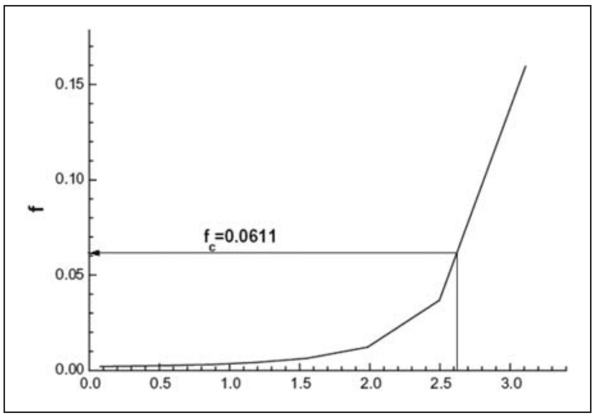

Figure 2. Determination of f_c.[29]

the plastic limit load model initially developed by Thomason.[2] Rakin[28–30] has determined the parameter f_c from an axisymmetric smooth specimen test. The critical values were determined based on the bisection of the formed curves and the straight line corresponding to the value of the diameter reduction at failure. This simple procedure seems to be closer to practical application than 'adjustment' (fitting) of numerical curves with the experimental ones for f–Δd diagram (Figure 2). On the other hand, the final failure VVF, f_F, is considered a parameter that may be experimentally determined.[31] Even though the VVF at final fracture, f_F, has been considered as an unimportant parameter, it is interesting to know whether it is constant.[14] The increases in porosity may in general have contributions from two processes: the growth of existing voids and the nucleation of new voids. Mathematically this can be expressed as

$$\dot{f} = \dot{f}_{growth} + \dot{f}_{nucleation} \tag{4}$$

Assuming that the matrix is plastically incompressible; the growth part is directly related to the mesoscopic plastic dilatation

$$\dot{f}_{growth} = (1 - f)\dot{\varepsilon}^p_{kk} \tag{5}$$

where $\dot{\varepsilon}^p_{kk}$ is the trace of the macroscopic plastic strain rate tensor. Void nucleation based on plastic straining can be included by

$$\dot{f}_{nucleation} = A\dot{\bar{\varepsilon}}^p \tag{6}$$

The parameter 'A' follows a normal distribution, as suggested in Chu and Needleman[32] and Tvergaard and Needleman[33]

$$A = \frac{f_N}{S_N\sqrt{2\pi}} \exp\left[-\frac{1}{2}\left(\frac{\bar{\varepsilon}^p - \varepsilon_N}{S_N}\right)^2\right] \tag{7}$$

Growth of porosity due to the nucleation voids introduces the parameter 'A' in equation (7); ε_f is the mean void nucleation strain, S_N the standard deviation of the distribution and f_N the volume fraction of particles available for void nucleation. The description of this stage needs the determination of these three parameters. Generally, ε_N and S_N values are, respectively, 0.3 and 0.1 for most materials. Thus, they can be considered as constants of the statistical distribution law and not as intrinsic material characteristics. The parameter f_N, which is commonly interpreted as the volume fraction of 'void nucleating particles' may only be identified with the total volume fraction of the inclusions for debonding particles where the initial void contains the whole particle.[34] The difficulty for modelling this problem is in introducing the nucleation of voids at cracked particles. An empirical approach was introduced in Chu and Needleman[32] to describe a normally distributed nucleation density function of the three parameters, f_N, ε_N and S_N.

Void growth may be treated independent of the material (hardening); however, void nucleation is a highly material-dependent process. This justifies the fact that void nucleation is the least understood part of ductile fracture. Void nucleation belongs to material intrinsic properties and governs the material failure behaviour. In general, it depends on particle strength, size and shape and the hardening exponent of the matrix material. The nucleation mechanism can be controlled by strain, or by stress; in this last case, the hydrostatic tension stress plays an important role.[34]

A great deal of experimental work has been performed to quantify void nucleation and growth. In general, these studies involved the use of both smooth and notched tensile specimens.[32–39] The quantification of the VVF is made by both optical methods[40,41] and Archimedes' principle.[42–46] Modelling of the first phase of ductile fracture – void nucleation – has been carried out using quantitative metallographic analysis of non-metallic inclusion content in tested steel.[29] Lievers et al.[47] proposed a novel method for the quantification of void nucleation rates in sheet material. An incremental sheet forming process is used to create large regions of homogeneous deformation, such that material density variations can then be used to quantify the evolution of VVF with the applied strain.

One of the most popular and convenient ways to model the nucleation, growth and coalescence of voids in a continuum FE method formulation is the use of Gurson–Tvergaard–Needleman (GTN) constitutive softening equations. In the GTN model, nucleation is most commonly seeded using the normal distribution scheme originally proposed by Chu and Needleman.[32] Huber et al.[48] developed a micromechanical model for the ductility of plastically deforming materials containing a homogeneous distribution of brittle inclusions for aluminium alloys. The model includes a micro–macro void nucleation condition with initial penny shape nature of the voids and also the growth and coalescence regimes. The model was validated by comparing the numerical predictions to the experimental results obtained under different levels of stress triaxiality and for different heat treatments controlling the hardness of the matrix.

In this article, the GTN template parameter identification methodology is proposed to describe the ductile fracture of metals. Adjustment settings of q_1 and q_2 are set to 1 and 1.5. Similarly, ε_N and S_N nucleation settings are set to 0.3 and 0.1. The initial volume fraction is considered a metallurgical characteristic of the initial state of the material. It is obtained by measuring and in our case the value is equal to 10^{-5} for 12NiCr6 steel. This value is located in the low values of the f_0 range. Assumptions consider the f_F is a parameter that characterises the end of the process of failure and its value can be approximately in the range 10–20%. Thus, our study is focused on the effect of two principal parameters, f_N and f_c, on the behaviour of the fracture strain by a tensile test performed on a axisymmetric notched bar AN2.

The initial VVF is obtained from experimental observations and its value is $f_0 = 1e^{-5}$. The final VVF is as a result of a calibration procedure.

The other parameters are set as follows: $q_1 = 1.5$, $q_2 = 1$, $\varepsilon_N = 0.3$ and $S_N = 0.1$.

Materials and experimental procedure

Materials

The nickel and chromium steel used in this study is the 12NiCr6 steel. Its chemical composition is given in
6 Table 1. The steel was austenitised at 880°C f_{time} of or 1 h, and then quenched in an oven. The initial VVF, f_0, is small ($f_0 = 10^{-5}$). This micro-structural parameter is necessary to use the GTN model. The principal mechanical characteristics are carried out from three tensile tests of smooth round bar with 11 mm diameter (Figure 3). These properties are summarised in Table 2.

Experimental procedure

Tensile tests have been conducted on axisymmetric notched tensile bar AN2 (Figure 4) to establish the
7 load–diametral contraction curve. During this kind of test, it is difficult to correctly measure the diameter contraction. In our study, the variation of the diameter has been measured using an image technique, which has the advantage of not requiring contact. An example of an image is shown in Figure 5. This technique follows the evolution of the diameter reduction exactly at the notch bottom and at the minimum diameter. In addition, the image analysis technique easily detects the point where crack initiation is localised. Figure 6 shows the evolution of the applied load as a function of diameter reduction Δd_c for the notched round tensile bar with 2 mm radius (AN2). At point 'P', there is a sharp change in the slope and a drastic fall in load, showing the initiation of failure process. This point gives the critical diameter reduction, Δd, at crack initiation. The ductility ε_f is defined as the average longitudinal strain at fracture

$$\varepsilon_f = 2\ln\left(\frac{d_0}{d_0 - \Delta d_c}\right) \tag{8}$$

$d_0 = 6$ mm is the initial diameter at the notch.

In our experimental test, $\Delta d_c = 1.6$ mm and so $\varepsilon_{f(experiment)} = 0.62$.

Table 1. Chemical composition of the 12NiCr6 steel.

C	S	Si	Mn	Ni	Cr	Al	14
0.12	0.007	0.032	0.6	1.6	0.85	0.176	

FE analysis

Detailed elastic–plastic, axisymmetric FE damage analyses based on the GTN model, described in 'Materials and experimental procedure', were performed to simulate tensile tests of smooth and notched round bars using ABAQUS/Explicit.[49] To incorporate a large geometry change effect, the large geometry change option was chosen.

A velocity $v(t)$ boundary condition was applied to the top of the FE model. In the quasi-static case, a
0.33 mm/min value was chosen. The resulting tensile 8
load was determined from nodal forces. Axisymmetric conditions are imposed on the bottom and the left. Gauge length elongation was also monitored from the FE displacement results. The four-node solid element with reduced integration within ABAQUS/Explicit 6.5 (element type CAX4R) was used. It should be noted that the element size could be important in FE damage analysis. Convergence tests were performed in order to optimise the CPU time and consequently the number of elements and nodes in FE meshes are 660 elements/725 nodes to nodes, depending on a notch radius. Typical FE meshes, employed in this study are shown in Figure 7.

Results and discussion

A parametric study of Gurson was carried out in order to show the effect of various parameters on the breakpoint of load–diametral contraction curve, F–Δd, of an axisymmetric notched tensile bar AN2. The parameters for this point are essential to have the best fit between the numerical and experimental curves. The aim is to propose a methodology to determine the best set of parameters.

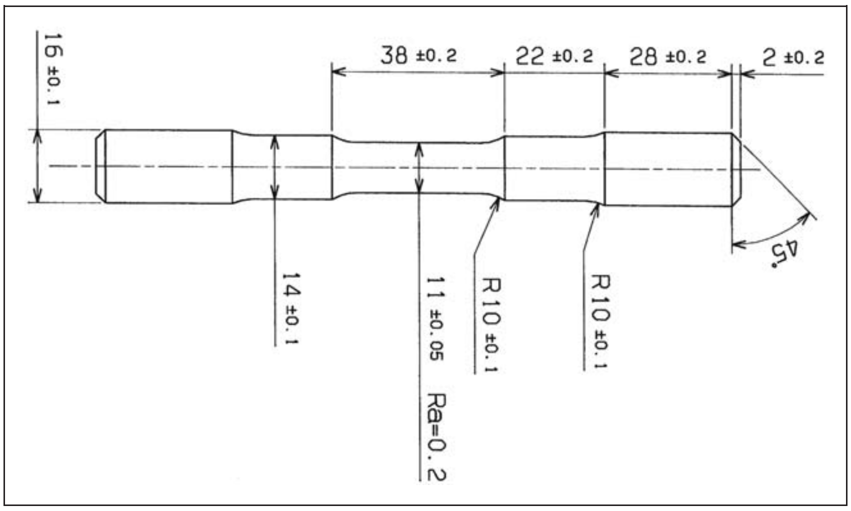

Figure 3. Smooth tensile bar.

Table 2. Mechanical properties of the 12NiCr6 steel.

E (GPa)	σ_y (MPa)	E/σ_y	σ_{max} (MPa)	*A* (%)	*Z* (%)	*n*	*k* (MPa)
194	340	570	489	31.2	49	0.45	544

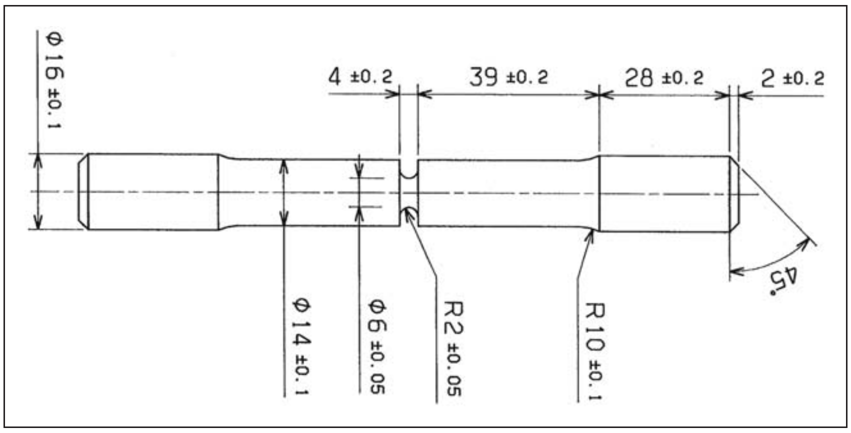

Figure 4. Notched round tensile bar with 2 mm radius (AN2).

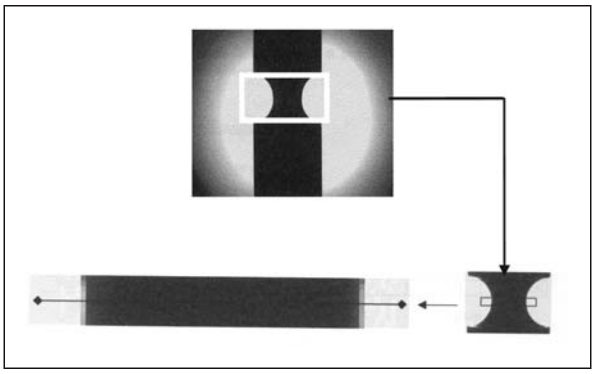

Figure 5. Measure of diametral contraction by image technique.

Figure 8 presents the combined effect of the nucleation parameter f_N and the critical parameter f_c on the load–diametral contraction curve. We note that these two parameters strongly influence the increase of fracture strain ε_f. It believes inversely with the nucleation 9 VVF of f_N. We also analyse the combined effect of each couple of parameters on the curve adjustment. This analysis shows that value quarters between f_N and f_c destabilise the numerical model's response, as shown in Figure 9. A gap must be maintained between the two parameters to avoid instability or divergence of the calculation process. These same remarks are valid between f_0 and f_N and between f_c and f_F.

Figure 10 summarises the precedent results. Shaded areas represent areas of divergence. This dictated the

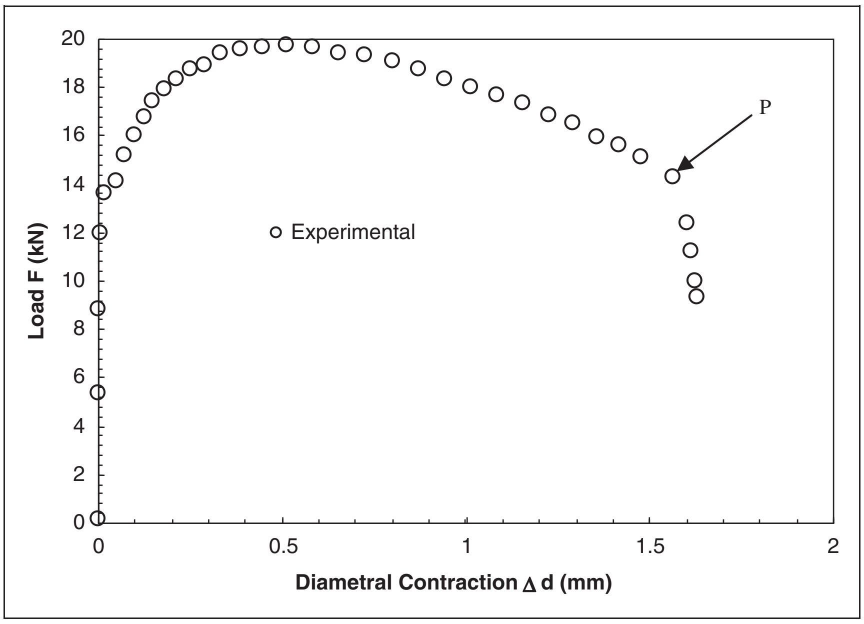

Figure 6. Load vs. diameter contraction of notched axisymmetric specimen test AN2.

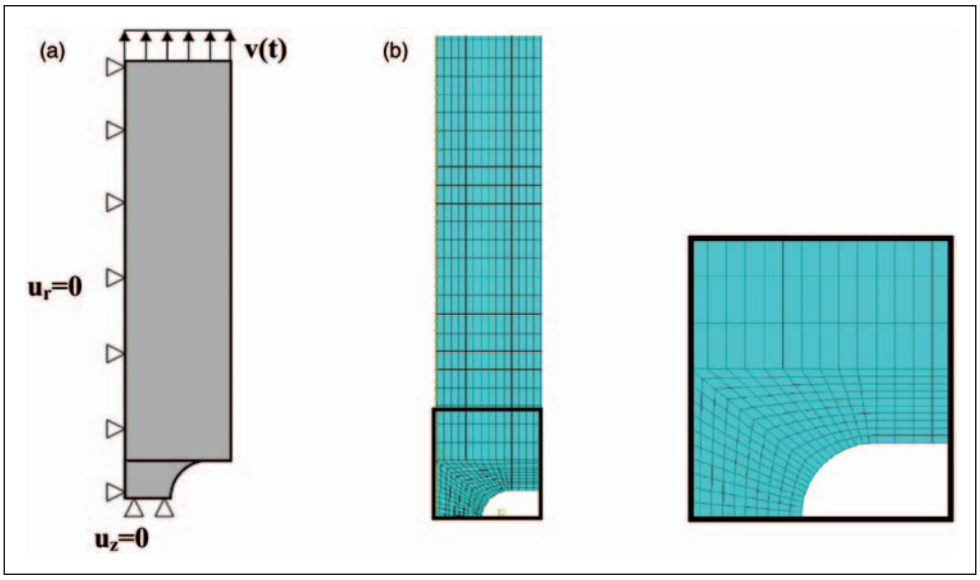

Figure 7. FE model for AN2 notched axisymmetric tensile bar: (a) boundary conditions; (b) mesh.
FE: finite element.

choice of intervals of different parameters of the parametric study.

Determination of f_N and f_c parameters

The angular point load–diametral contraction curve, F–Δd, represents a sudden load drop. This point gives us the critical failure diameter. Corresponding deformation calculated from equation (8) represents the strain fracture or ductility. A parametric study (Figure 11) allows, for a given f_0, to plot a series of curves for different values of f_c.

Then, by drawing a family of curves $f_c(\varepsilon_f)$ for varying f_0, we can quantify the effect of f_0 on ε_f. (Figure 12) We note that for the materials with low initial porosity, as 12NiCr6 steel, the effect of this parameter is not important.

From this observation, determination method can be applied from the $f_c(\varepsilon_f)$ curve for the value $f_0 = 1e{-}5$, representing the initial porosity 12NiCr6 steel.

For determination of f_c value, experimental result of fracture strain $\varepsilon_{f(experiment)}$ was used, at which sudden drop of force occurs, which is caused by coalescence of voids in the material (Figure 8). The value obtained is $f_c = 0.06$ (Figure 13).

The term f_N is determined by delaying experimental value of fracture strain on the $f_N(\varepsilon_f)$ curve for $f_c = 0$

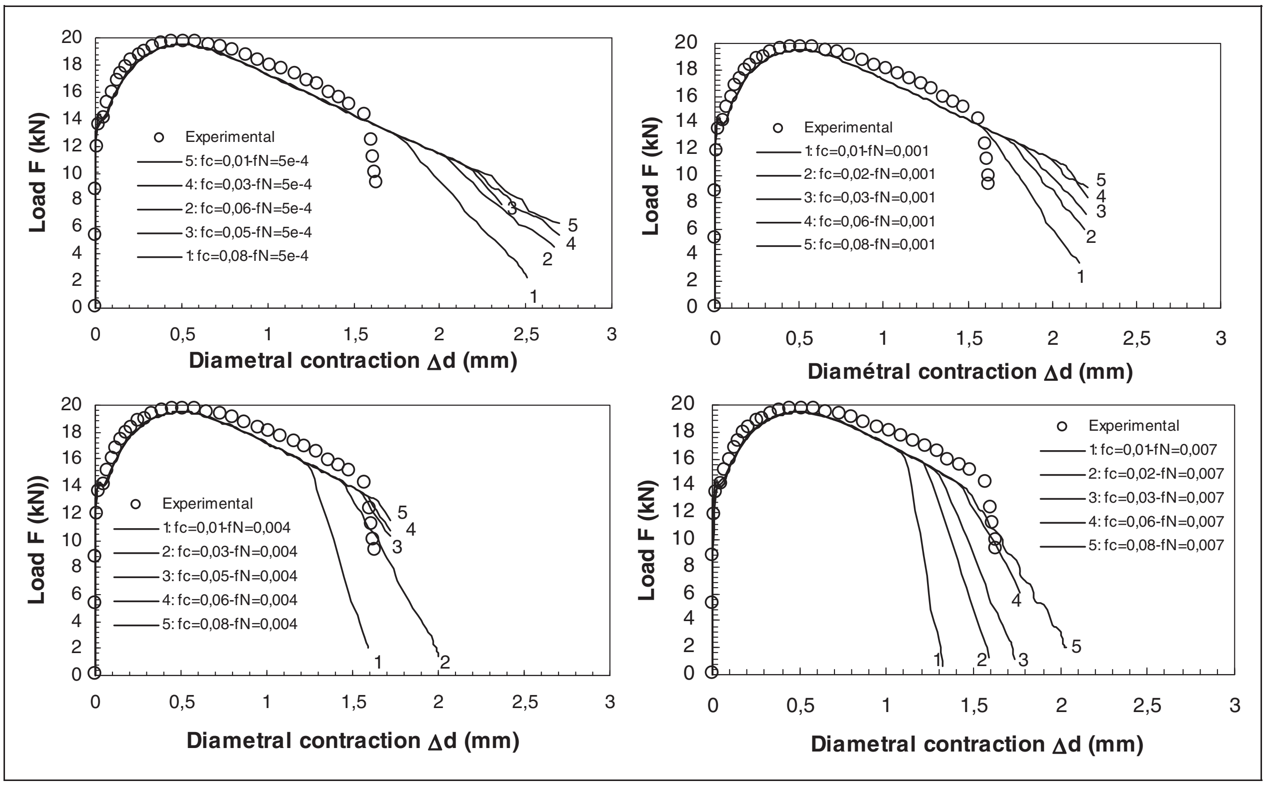

Figure 8. Combined effect of the f_N and f_c parameters on the load–diametral contraction curve.

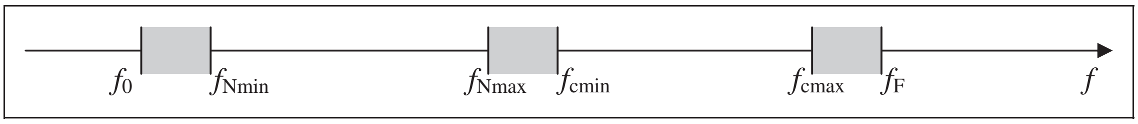

Figure 9. Schematic representation of the parameter range.

06 curve. From this graphical construction, we deduce the value of $f_N = 0.0039$ (Figure 13).

Effect of f_N and f_c parameters on the VVF variation

Figure 14(a) shows the evolution of the VVF or porosity in the centre of the specimen. It is strongly influenced by the volume fraction in the nucleation f_N. For a low level of nucleation, the final volume fraction, f_F, i.e. the failure initiation reaches the high rates of plastic strain. However, for higher values of f_N, a smaller plastic strain is sufficient.

Figure 14(b) shows that the critical volume fraction, f_c, especially affects the coalescence acceleration. For low values of f_c, the final volume fraction is reached faster.

Effect of f_N and f_c parameters on the equivalent plastic strain

Figures 15 and 16 show the effect of f_N on the changes in the critical VVF f_c based on the equivalent plastic strain in the specimen centre. We also note that for low initial porosities the critical volume fraction f_c varies a little according to the equivalent plastic deformation. (Figure 17).

Visualisation of the crack propagation using GTN model

Figure 18 shows the area where the final volume fraction is reached at the striction line, thus we can materialise the failure area. These elements are completely losing their rigidity and volume fraction reaches its final value. The Gurson model crack propagation described in this way.

Conclusion

The difficulty in the application of the GTN model lies in the following points:

- the significant number of parameters for identification
- no unique set of the parameters allowing fitting of the numerical curve on the experimental one.

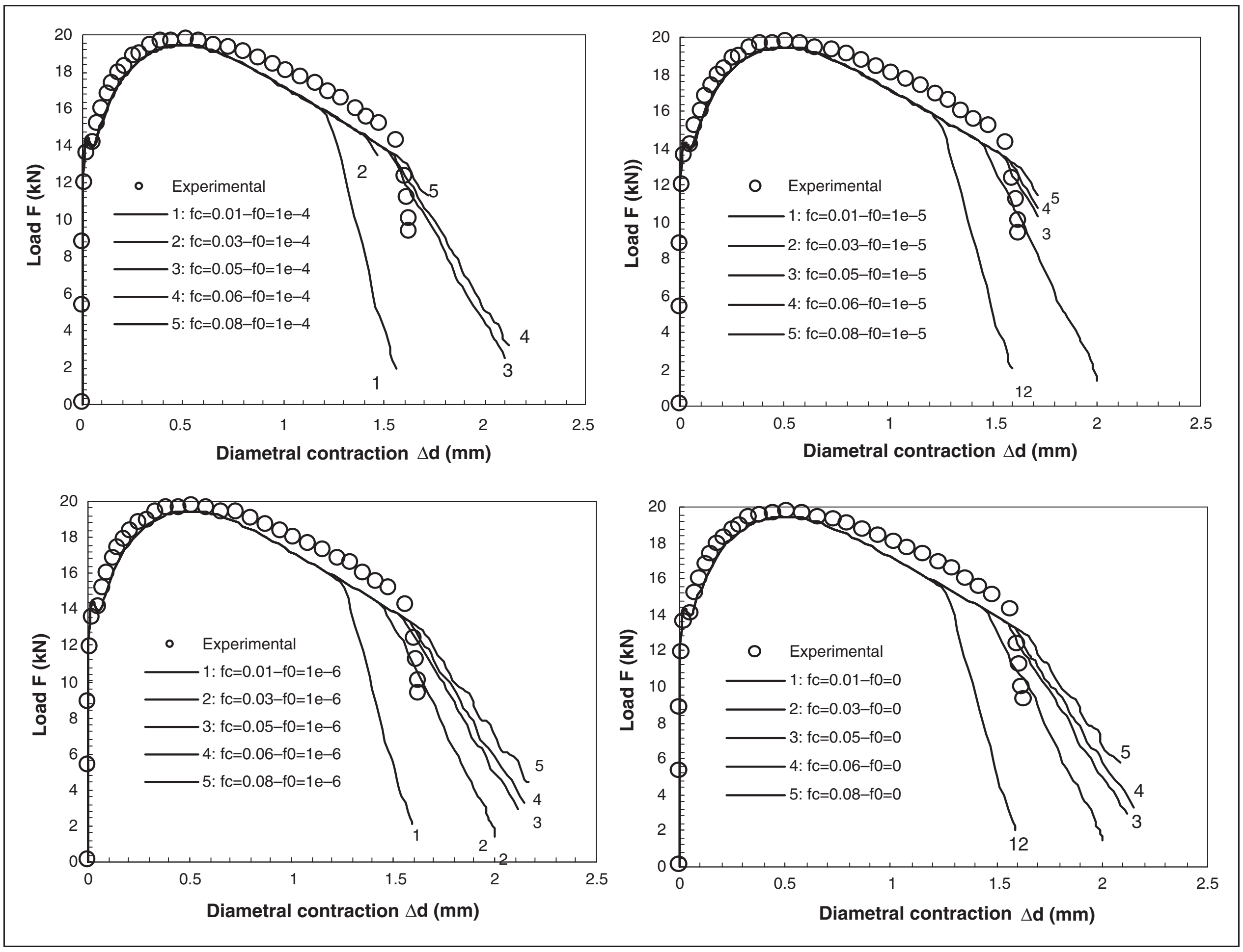

Figure 10. Effect of f_0 load vs. diametral contraction.

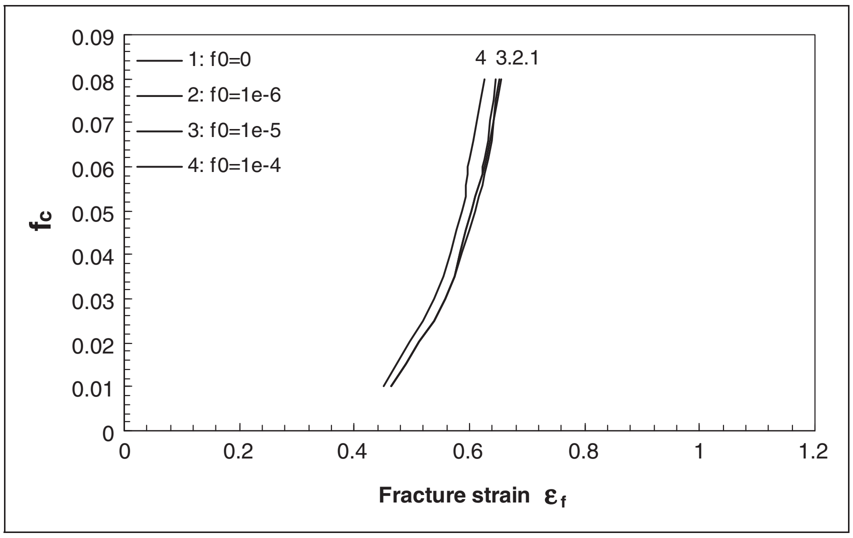

Figure 11. Initial porosity vs. fracture strain.

In this article, we proposed a method which consists to lie the parameters of nucleation f_N and of beginning of coalescence f_c with physical parameters such as the initial VVF f_0 and the strain at failure ε_f. This method makes it possible to solve the unique problem of the parameter set.

This article presents a phenomenological model of ductile fracture for the 12NiCr6 steel using the GTN model. Experimental tests and FE damage simulations using the GTN model are performed for smooth and notched tensile specimens from which the parameters in the GTN model are calibrated.

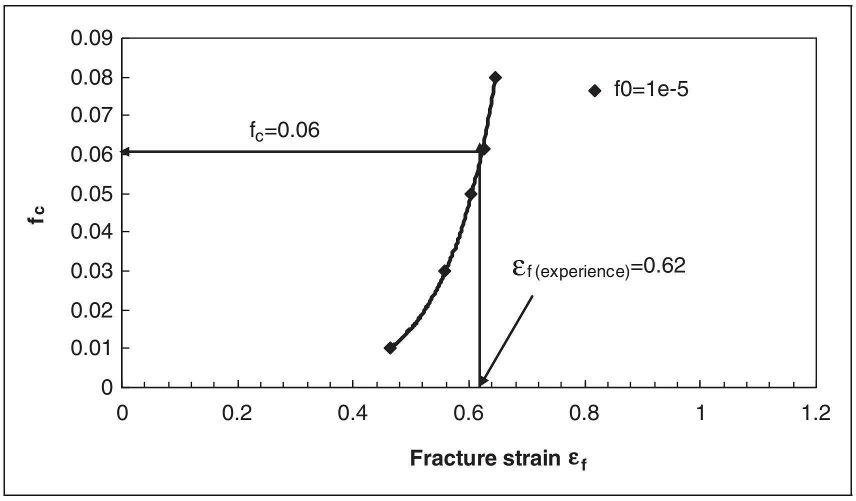

Figure 12. Identification of f_c.

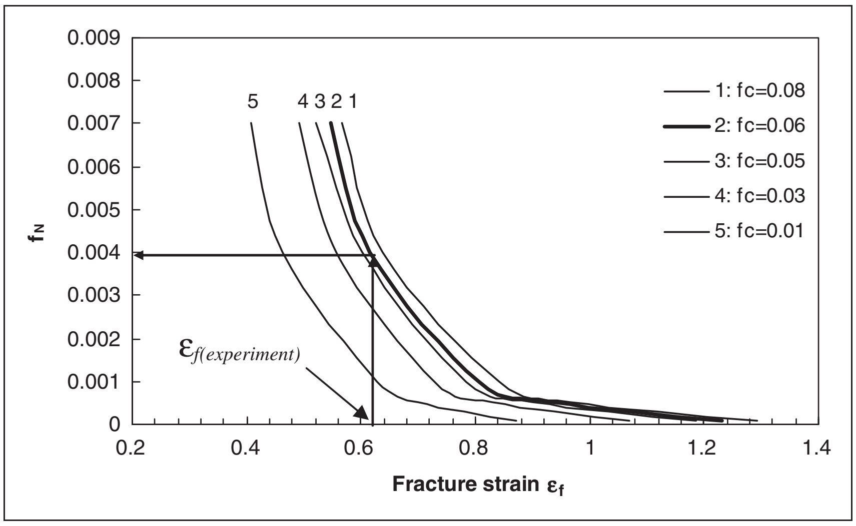

Figure 13. Nucleation VVF vs. fracture strain f_c effect.
VVF: void volume fraction.

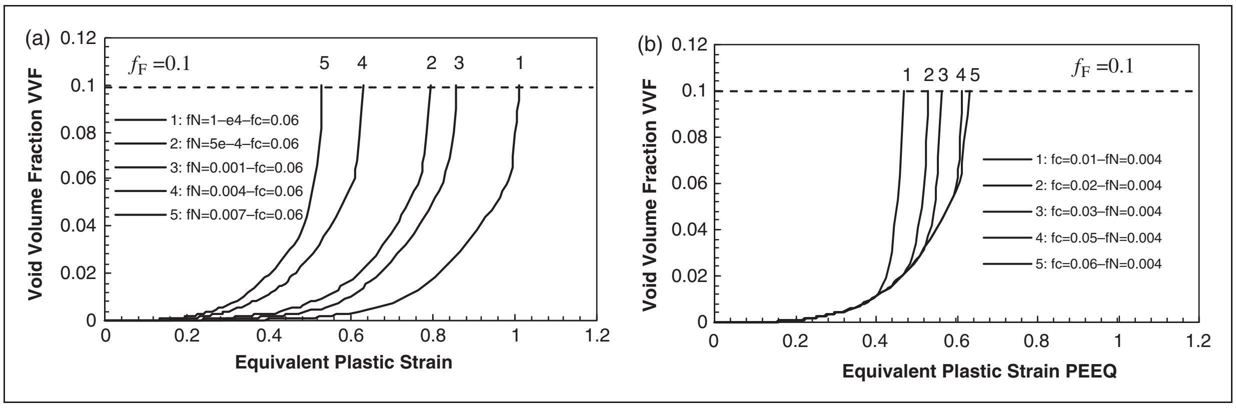

Figure 14. VVF variation in the specimen centre: (a) f_N effect; (b) f_c effect.
VVF: void volume fraction.

An approach to parameter identification of the GTN model was presented using force–diametral contraction curves of axisymmetric notched specimen Validity of the proposed parameters is checked by comparing the simulated results with the experimental ones from the notched bar. The dependence between the parameters of the GTN model and strain at failure ε_f was highlighted by studying the variations of

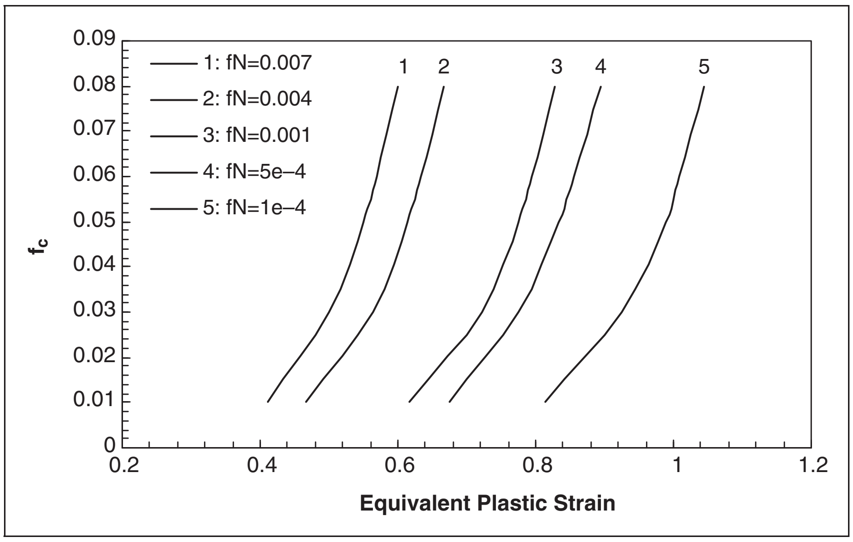

Figure 15. Effect of f_N on the f_c vs. equivalent plastic strain.

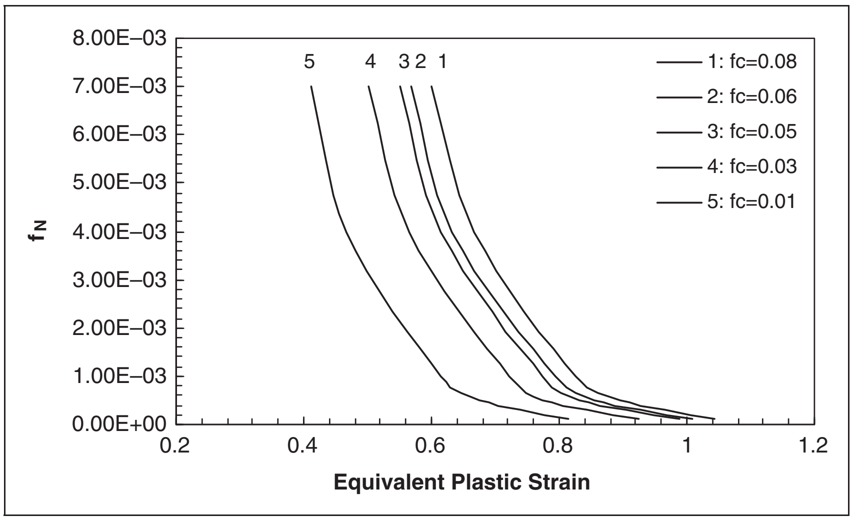

Figure 16. Effect of f_c on the f_N vs. equivalent plastic strain.

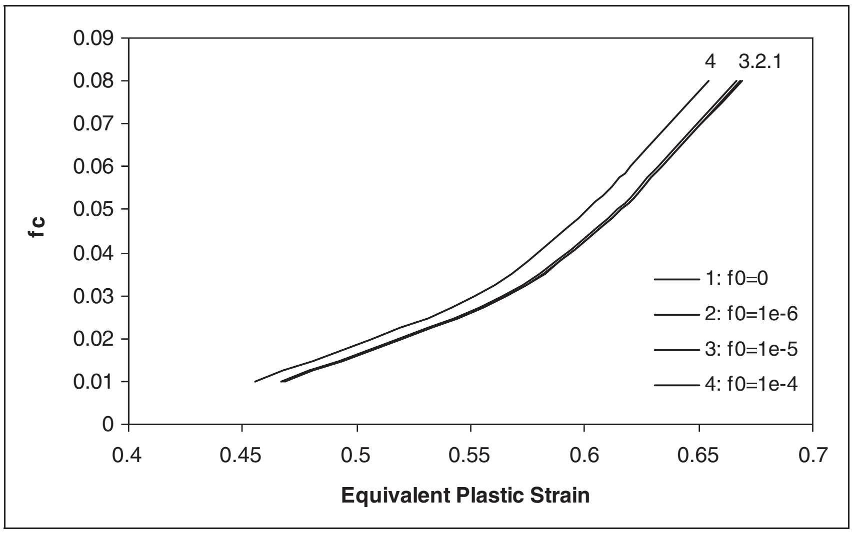

Figure 17. Effect of f_0 on the f_c vs. equivalent plastic strain.

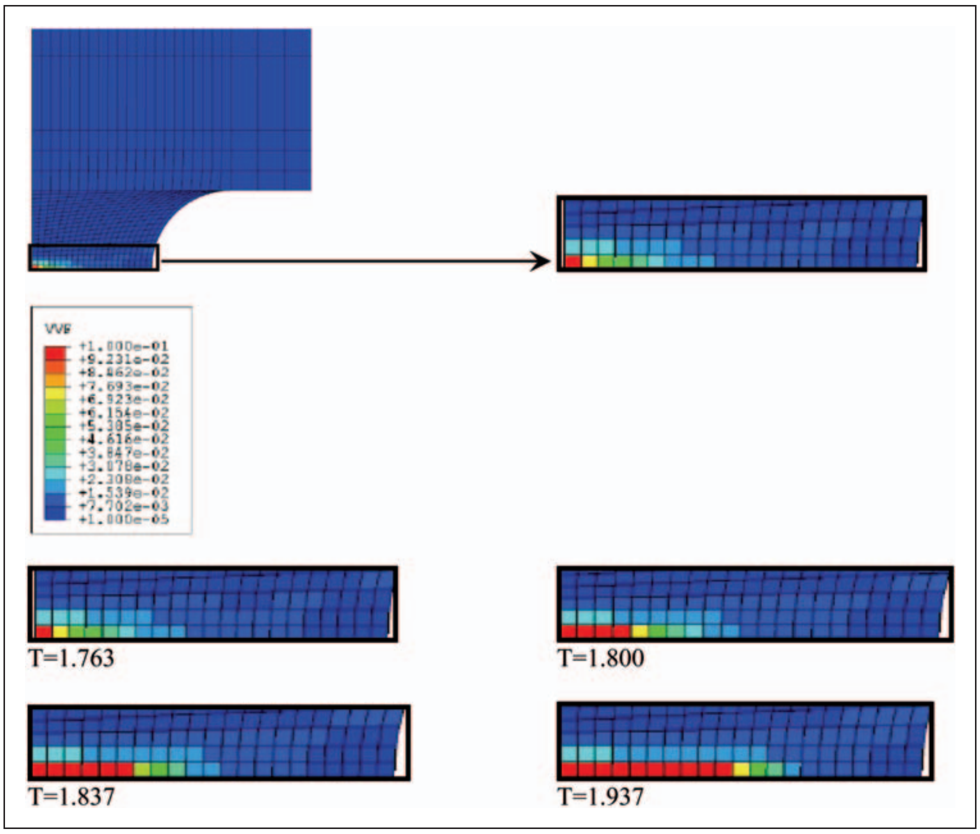

Figure 18. Visualisation of the crack propagation by GTN model.
GTN: Gurson–Tvergaard–Needleman.

parameters f_c and f_N depending on strain at failure ε_f. From the graphs $f_N(\varepsilon_f)$ and $f_c(\varepsilon_f)$, we were able to identify the parameters of the critical volume fraction, f_c, and the nucleation volume fraction f_N. This approach allowed us to determine the critical volume fraction and nucleation for steel 12NiCr6, which are $f_c = 0.06$ and $f_N = 0.004$. The influence of triaxiality on the parameters is a very important aspect of the identification problem. This study was conducted on the notched tensile bar AE2, so for one triaxiality. A similar study on other specimens with different notch radii, i.e. different triaxialities is necessary. Influence of the volume rate of inclusions which characterises the initial porosity depends on the type of alloy to be considered. To complete the study, a validation on cracked specimens is necessary.

Funding

The authors extend their appreciation to the Deanship of Scientific Research at King Saud University for funding the study through the research group no. RGP-VPP-035.

References

1. Hancock JW and Mackenzie AC. On the mechanisms of ductile failure in high-strength steels subjected to multi-axial stress-states. *J Mech Phys Solids* 1976; 24(2–3): 147–160.
2. Thomason PF. *Ductile fracture of metals*. Oxford: Pergamon Press, 1990.
3. Gurson AL. Continuum theory of ductile rupture by void nucleation and growth. Part 1 – yield criteria and flow rules for porous ductile media. *J Eng Mater Technol* 1977; 99: 2–15.
4. Rice JR and Tracey DM. On the ductile enlargement of voids in triaxial stress fields. *J Mech Phys Solids* 1969; 17: 201–207.
5. McClintock FA. A criterion of ductile fracture by the growth of holes. *J Appl Mech* 1968; 35: 363–371.
6. Tvergaard V. Influence of voids on shear band instabilities under plane strain conditions. *Int J Fract* 1981; 17: 389–407.
7. Tvergaard V. On localization in ductile materials containing spherical voids. *Int J Fract* 1982; 18: 237–252.
8. Perrin G and Leblond JB. Analytical study of a hollow sphere made of plastic porous material and subjected to hydrostatic tension—application to some problems in ductile fracture metals. *Int J Plast* 1990; 6: 677–698.
9. Faleskog J, Gao X and Shih CF. Cell model for nonlinear fracture mechanics—I. Micromechanics calibration. *Int J Fract* 1998; 89: 365–373.
10. Steglich D and Brocks W. Micromechanical modelling of damage and fracture of ductile materials. *Fatigue Fract Eng Mater Struct* 1998; 21(10): 1175–1188.
11. Ragab AR. Application of an extended void growth model with strain hardening and void shape evolution to ductile fracture under axisymmetric tension. *Eng Fract Mech* 2004; 71: 1515–1534.
12. Vadillo G and Fernández-Sáez J. An analysis of Gurson model with parameters dependent on triaxiality based on unitary cells. *Eur J Mech A. Solids* 2009; 28: 417–427.

13. Dutta BK, Guin S, Sahu MK, et al. A phenomenological form of the q2 parameter in the Gurson model. *Int J Press Vessels Pip* 2008; 85: 199–210.
14. Zhang ZL and Niemi E. A new failure criterion for the Gurson–Tvergaard dilatation constitutive model. *Int J Fract* 1995; 70: 321–334.
15. Steglich D and Brocks W. Micromechanical modelling of damage and fracture of ductile materials. *Fatigue Fract Eng Mater Struct* 1998; 21(10): 1175–1188.
16. Koplik J and Needleman A. Void growth and coales-
11 cence in porous plastic solids. *Int J Solids Struct* 1988; 24: 835–853.
17. Kuna M, Sun D-Z. Analysis of void growth and coalescence in cast iron by cell models. In: *1st European mechanics of materials conference on local approach to fracture '86–96'*, Fontainebleau, France, 9-11 September 1996.
18. Brocks W, Sun DZ and Hönig A. Verification of the transferability of micromechanical parameters by cell model calculations with visco-plastic materials. *Int J Plast* 1995; 11(8): 971–989.
19. Sun D-Z, Siegele D, Voss B, et al. Application of local damage models to the numerical analysis of ductile rupture. *Fatigue Fract Eng Mater* 1989; 12(3): 201–212.
20. Sun D-Z, Voss B and Schmitt W. Numerical prediction of ductile fracture resistance behaviour based on micromechanical models. In: JG Blauel and KH Schwalbe (eds) *Defect assessment in components – fundamentals and applications (ESIS/EGF9)*. London: Mechanical Engineering Publications, 1991, pp.447–458.
21. Sun D-Z, Kienzler R, Voss B, et al. Application of micro-mechanical models to the prediction of ductile
12 fracture. fracture mechanics. In: SN Atluri (ed.) *22nd Symposium (Volume II), ASTM STP 1131*. Philadelphia, PA: American Society for Testing and Materials, 1992, pp.368–378.
22. Bernauer G, Brocks W. Numerical, round robin on micro-mechanical models: conclusions of part A (ductile tearing) and first results of part B (cleavage fracture). In: *ESIS TC1 and TC8 meeting*, Statoil Research Centre, Trondheim, 26 August 1999.
23. Brocks W, Bernauer G. Determination of the Gurson parameters by numerical simulations. In: *2nd Griffith conference Sheffield*, UK, 13–15 September, 1995.
24. Oh C-K, Kim Y-J, Baek J-H, et al. A phenomenological model of ductile fracture for API X65 steel. *Int J Mech Sci* 2007; 49: 1399–1412.
25. Pavankumara TV, Samala MK, Chattopadhyaya J, et al. Transferability of fracture parameters from specimens to component level. *Int J Press Vessels Pip* 2005; 82: 386–399.
26. Zhang ZL, Thaulow C and Ødegård J. A complete Gurson model approach for ductile fracture. *Eng Fract Mech* 200l; 67: 155–168.
27. Acharyya S and Dhar S. A complete GTN model for prediction of ductile failure of pipe. *J Mater Sci* 2008; 43: 1897–1909.
28. Rakin M, Cvijović Z, Grabulov V, et al. Micromechanism of ductile fracture initiation: void nucleation and growth. *Facta Univer Ser: Mechanical Engineering* 2000; 1(7): 825–833.
29. Rakin M, Cvijović Z, Grabulov V, et al. Prediction of ductile fracture initiation using micromechanical analysis. *Eng Fract Mech* 2004; 71: 813–827.
30. Rakin M, Gubeljak N, Dobrojević M, et al. Modelling of ductile fracture initiation in strength mismatched welded joint. *Eng Fract Mech* 2008; 75: 3499–3510.
31. 31. Bauvineau L, Burlet H, Eripret C, et al. Modelling ductile stable crack growth in a C-Mn steel with local approaches. In: *First European mechanics of materials conference on local approach to fracture*, Fontainebleau, France, 9–11 September 1996.
32. Chu CC and Needleman A. Void nucleation effects in biaxially stretched sheets. *J Eng Mater Technol* 1980; 102: 249–256.
33. Tvergaard V and Needleman A. Analysis of the cup-cone fracture in a round tensile bar. *Acta Metall* 1982; 32: 157–169.
34. Zhang ZL. A complete Gurson model. In: MH Alibadi (ed.) *Nonlinear fracture and damage mechanics*. Southampton, UK: WIT Press, 2001, pp.223–248.
35. Steglich D and Brocks W. Micromechanical modelling of the behaviour of ductile materials including particles. *Comput Mater Sci* 1997; 9: 7–17.
36. Beremin FM. Cavity formation from inclusions in ductile fracture of A508 steel. *Metall Trans A* 1981; 12: 723–731.
37. Guillemer-Neel C, Feaugas X and Clavel M. Mechanical behavior and damage kinetics in nodular cast iron: Part I. Damage mechanisms. *Metall Mater Trans A* 2000; 31: 3063–3074.
38. Kwon D and Asaro RJ. A study of void nucleation, growth, and coalescence in spheroidized 1518 steel. *Metall Mater Trans A* 1990; 21: 117–134.
39. Agarwal H, Gokhale AM, Graham S, et al. Void growth in 6061-aluminum alloy under triaxial stress state. *Mater Sci Eng A* 2003; 341: 35–42.
40. Cox T and Low JJ. An investigation of the plastic fracture of AISI4340 and 18Nickel-200 grade maraging steels. *Metall Trans A* 1974; 5: 1457–1470.
41. Brownrigg A, Spitzig W, Richmond O, et al. The influence of hydrostatic pressure on the flow stress and ductility of a spheroidized 1045 steel. *Acta Metall* 1983; 31: 1141–1150.
42. Barlat F and Jalinier J. Formability of sheet metal with heterogeneous damage. *J Mater Sci* 1985; 20: 3385–3399.
43. Brathe L and Scand J. Macroscopic measurements of creep damage in metals. *J Metall* 1978; 7: 199–203.
44. Rosowski A and Olejnik L. Damage evolution in mild steel. *Int J Mech Sci* 1988; 30: 51–60.
45. Spitzig WA. Effect of hydrostatic pressure on deformation, damage evolution, and fracture of iron with various initial porosities. *Acta Metall Mater* 1990; 38: 1445–1453.
46. Koenigsmann HJ, Starke Jr EA and Allaire PE. Finite element/experimental analysis of cavity nucleation in an Al-Si-Ge alloy. *Acta Mater* 1996; 44: 3069–3075.
47. Lievers WB, Pilkey AK and Lloyd DJ. Using incremental forming to calibrate a void nucleation model for automotive aluminum sheet alloys. *Acta Mater* 2004; 52: 3001–3007.
48. Huber G, Brechet Y and Pardoen T. Predictive model for void nucleation and void growth controlled ductility in quasi-eutectic cast aluminium alloys. *Acta Mater* 2005; 53: 2739–2749.
49. ABAQUS version 6.5. User's manual. Hibbitt, Karlsson & Sorensen Inc., 2005.

50. Lemaitre J. Coupled elasto-plasticity and damage constitutive equations. *Comput Meth Appl Mech Eng* 1984; 51: 31–49.
51. Oyane M, Sato T, Okimoto K, et al. Criteria for ductile fracture and their applications. *J Mech Work Technol* 1979; 4: 65–81.
52. Beremin FM. Experimental and numerical study of the different stages in ductile rupture: application to crack initiation and stable crack growth. In: S Nemat-Nasser (ed.) *Three-dimensional constitutive relations and ductile fracture*. Amsterdam: North-Holland, 1981, pp.85–205.
53. Rousselier G. Ductile fracture models and their potential in local approach of fracture. *Nucl Eng Des* 1987; 105: 97–111.
54. Rice JR and Tracy DM. On the ductile enlargement of voids in triaxial stress fields. *Int J Mech Phys Solids* 1969; 17: 201–217.